Weather and Climate Extremes 26 (2019) 100224

Contents lists available at ScienceDirect

Weather and Climate Extremes

journal homepage: http://www.elsevier.com/locate/wace

Saharan air intrusions as a relevant mechanism for Iberian heatwaves: The record breaking events of August 2018 and June 2019

Pedro M. Sousa [a,*], David Barriopedro [b], Alexandre M. Ramos [a], Ricardo García-Herrera [b,c], Fátima Espírito-Santo [d], Ricardo M. Trigo [a,e]

[a] Instituto Dom Luiz (IDL), Faculdade de Ciências, Universidade de Lisboa, 1749-016 Lisboa, Portugal
[b] Instituto de Geociencias, IGEO (CSIC-UCM), Spain
[c] Departamento de Física de la Tierra y Astrofísica, Facultad de Ciencias Físicas, Universidad Complutense de Madrid, Spain
[d] Instituto Português do Mar e da Atmosfera, Portugal
[e] Departamento de Meteorologia, Instituto de Geociências, Universidade Federal do Rio de Janeiro, Rio de Janeiro, 21941-916, Brazil

A B S T R A C T

The summers of 2018 and 2019 were characterized by unusually warm conditions over Europe. Here, we describe the intense heatwaves striking the Iberian Peninsula in early August 2018 and late June 2019. The 2018 episode was relatively short-lived but outstanding in amplitude, particularly in western Iberia. Similar to previous mega-heatwaves, the 2019 event was long-lasting and affected large areas of western and central Europe, including eastern Iberia. During these events, many absolute temperature records were broken in western and eastern Iberia, respectively (some of them standing since 2003). In both cases, a cyclonic circulation off the coast in the northeastern Atlantic and a strong subtropical ridge pattern over the affected area promoted the advection of an anomalously warm air mass. This paper highlights the role of these very warm, stable and dry air intrusions of Saharan origin in the western and eastern Iberia heatwave events. Using a thermodynamical classification based on the geopotential height thickness and potential temperature, we show how the magnitude and poleward extension of these Saharan intrusions were unprecedented in the period since 1948. The relationship between Iberian heatwaves and Saharan warm air intrusions is discussed in the long-term context, showing a closer link in southern sectors of the Peninsula. However, a consistent poleward trend in the latitudinal extension of these subtropical intrusions reveals their increasing relevance for heatwaves in northern sectors of Iberia and western Europe. This overall trend is accompanied by an apparent "see-saw" in the occurrence of subtropical intrusions between eastern and western Iberia on multi-decadal scales.

1. Introduction

Some of the most well studied exceptionally hot summers in recent years in Europe have been those of 2003 (Schär et al., 2004; García--Herrera et al., 2010) and 2010 (Barriopedro et al., 2011; Dole et al., 2011). In both cases, widespread above-average temperature anomalies were registered, and many new all-time temperature records were set at the time. They were associated with "mega-heatwaves" (Barriopedro et al., 2011; Miralles et al., 2014), which refer to outstanding heatwave (HW) events in terms of duration, intensity and spatial extent. The recent European HW event of June 2017 was the earliest summer mega-HW in the reanalysis period since1948 (Sánchez-Benítez et al., 2018). The end of June 2019 also saw an exceptional HW in central and western Europe. Despite occurring in the very early summer, large areas of France and Spain exceeded the temperatures registered during previous mega-HWs. The June 2019 HW had large repercussion on the media and, as it evolved before summer holidays, national governments activated contingency plans and deployed resources to minimize impacts (e.g. The Guardian, 2019). Over Iberia, the event was particularly severe in the eastern part, where some regions recorded absolute temperature records, whereas western Iberia experienced relatively milder conditions. Other recent summers, such as 2015 (Russo et al., 2015) and 2018, did not feature European mega-HWs, but did feature regional extreme events. During the summer of 2018, media coverage was particularly focused on persistent record-breaking temperatures in northernmost sectors of Europe. However, southwestern Europe was also struck by the occurrence of unprecedented temperature values during the first week of August. The intensity and relevance of the early August Iberian HW was masked by relatively wet and cool conditions in June and July 2018, resulting in near-average seasonal mean temperature anomalies in the region. Unprecedented absolute temperatures were recorded, particularly over Portugal, where all-time records were broken in many places, including most of those standing since the 2003 mega-HW (Instituto Português do Mar e da Atmosfera, hereafter IPMA, 2018).

Unlike the prolonged mega-HW events that occurred in August 2003

* Corresponding author.
E-mail address: ppsousa@fc.ul.pt (P.M. Sousa).

https://doi.org/10.1016/j.wace.2019.100224
Received 1 March 2019; Received in revised form 2 August 2019; Accepted 10 September 2019
Available online 14 September 2019

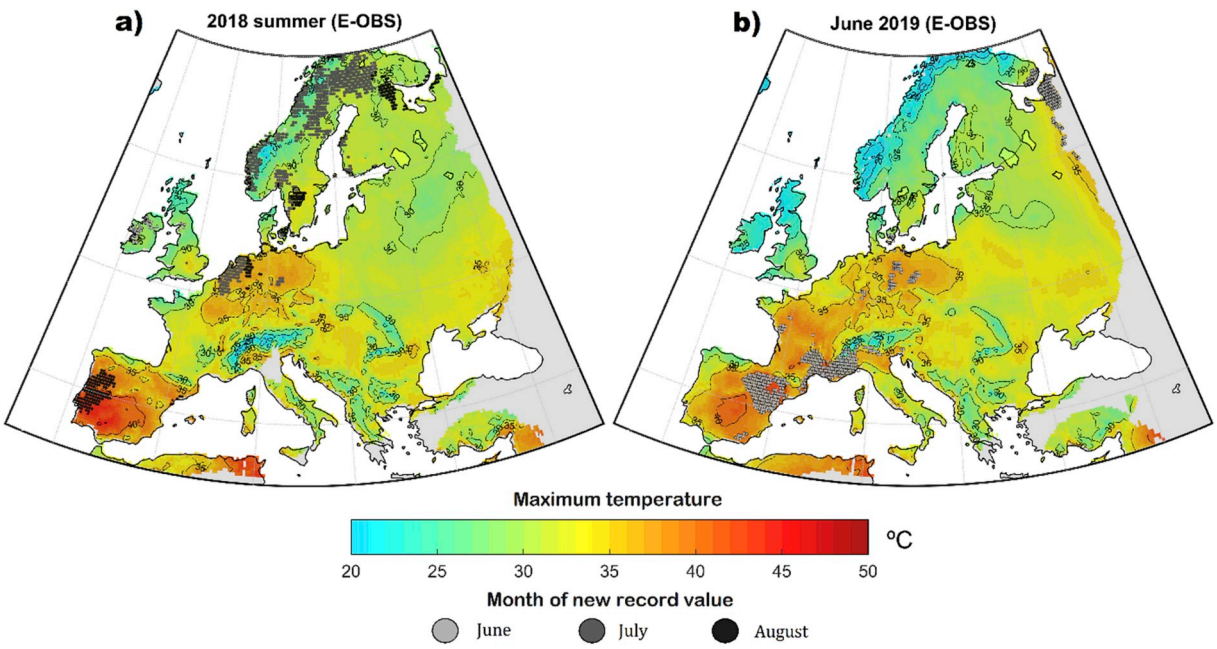

Fig. 1. Absolute maximum 2 m temperature (color shading) observed in Europe during: a) the 2018 summer (JJA); b) June 2019 according to the E-OBS gridded dataset. Hatched areas denote regions where new all-time maximum temperature records were set, with the grey scale denoting in which month the record occurred. (For interpretation of the references to color in this figure legend, the reader is referred to the Web version of this article.)

(Trigo et al., 2006) or June 2019, the early August 2018 heat episode was short-lived and more regional. Intense warm spells of this type display a more transient behavior than mega-HWs, which are associated with quasi-stationary pervasive anomalous conditions. In particular, local temperatures often exhibit abrupt increases that reach outstanding figures, being sometimes interrupted by non-extreme values. Mega-HWs and sharp HW events are difficult to diagnose from classical approaches, which follow a local perspective, often disregarding concomitant conditions in surrounding points and the discontinuous occurrence of extremes. Recent studies have proposed a semi-lagrangian approach that allows to identify nearby regions under HW conditions and track them in space and time (Sánchez-Benítez et al., 2018). This perspective provides a better frame to characterize the life-cycle of HWs and, in particular, the associated atmospheric circulation.

Regarding the synoptic conditions that led to the 2018 and 2019 HW events, a very warm air mass intrusion presenting dust concentrations (above normal daily reference levels) and originating from the Sahara led to weather warnings being issued by the national meteorological agencies, widely broadcasted in media with a few days in advance (Publico, 2018; El Tiempo Hoy, 2018; BBC, 2019). Among the distinct weather systems associated with HWs affecting Iberia (e.g. Garcia--Herrera et al., 2010), few studies have explicitly addressed Saharan warm air intrusions (hereafter SIs; e.g. Díaz et al., 2017). In fact, literature on SIs has mainly focused on their health impacts due to aerosol and dust transport (Salvador et al., 2014) and relatively less attention has been paid to their thermodynamical effects. As so, there is an incomplete description of the relationship between such air masses originated in the desertic region of northwestern Africa and HW episodes in Iberia. This is particularly notable in climatological studies, stressing the need of a historical record of SIs to characterize coherently their effects on the Iberian Peninsula (IP). Here we explore this issue, through relatively straightforward criteria for the detection of SIs based on air mass thermodynamical properties derived from meteorological reanalysis data. Accordingly, the main objectives of this work are:

1) Characterize the exceptionality of the extreme heat episodes that affected western and eastern IP in early August 2018 and late June 2019, respectively;
2) Describe the synoptic pattern and its spatio-temporal evolution during the events, with special emphasis on the occurrence of SIs, which are identified and tracked by designing an automatic algorithm;
3) Analyze the link between SIs and other Iberian HWs, as well as the long-term trends in the frequency of SIs affecting the Iberian Peninsula.

In Section 2 the Data and Methods employed in this work are presented. Section 3 characterizes the extreme episodes of August 2018 and June 2019, and its exceptionality when compared with previous episodes. In Section 4, we explore the life-cycle and unprecedented nature of the SI during each HW. Section 5 assesses the relationship between the occurrence of SIs and regional HWs in Iberia, as well as the long-term trends in the frequency of SIs. Finally, in Section 6 the main results are summarized and discussed.

2. Data and methods

2.1. Meteorological data

Daily maximum temperature series from the E-OBS gridded dataset were used to characterize extreme values and anomalies during the August 2018 and June 2019 events. E-OBS is an European land-only high-resolution gridded observational dataset, using the European Climate Assessment and Dataset (ECA&D) blended daily station data, and is presented on a horizontal resolution of $0.25^\circ \times 0.25^\circ$, starting from 1950 (Haylock et al., 2008). Here, files are replaced in monthly updates until each full update of the E-OBS dataset. Accordingly, small changes might occur between these releases, after new data and/or stations are added. The E-OBS data available until June 2019 was used here.

To better characterize the exceptionality of the more regional 2018 HW event, we also used maximum and minimum temperature series from continental weather stations provided by IPMA over the westernmost sector of the Peninsula, where it was more significant.

Meteorological fields were retrieved from the NCEP/NCAR reanalysis daily dataset (Kalnay et al., 1996) on a $2.5^\circ \times 2.5^\circ$ horizontal

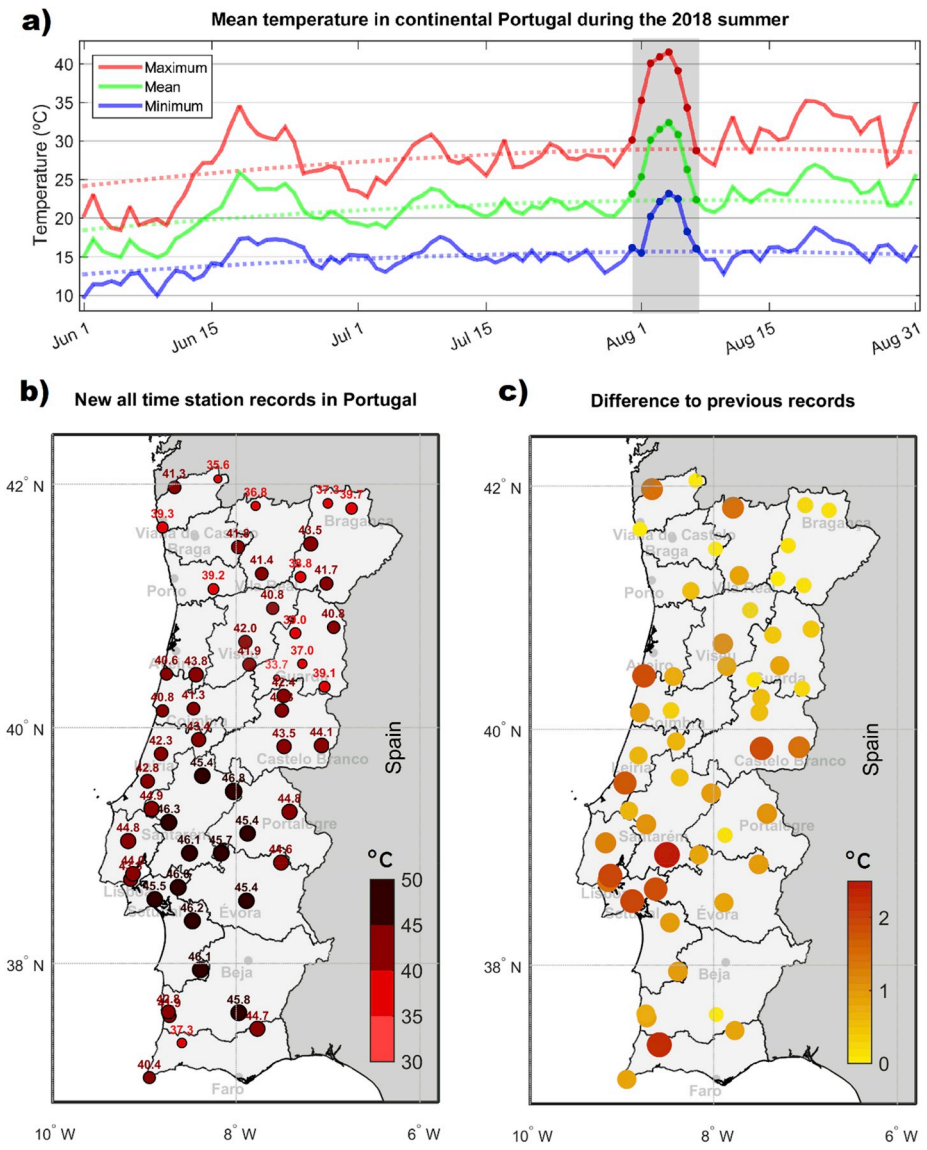

Fig. 2. a) Evolution of mean temperature in Portugal throughout the 2018 summer (thick lines), compared with the climatological mean (stippled lines), relying on IPMA surface stations. Highlighted values correspond to the dates enclosing the heat-wave event (as classified by IPMA, 1–6 August). b) New all-time temperature records (in °C) established during early August 2018 in surface stations in Portugal (IPMA). c) Difference (in °C) between the observed maximum temperatures during the event and the previous all-time records. Note that only stations with unprecedented values are presented.

resolution grid, starting from 1948. The following variables were considered for pressure levels between 1 000 and 500 hPa: air temperature, geopotential height, zonal/meridional wind components and vertical velocity. These fields were used to: i) characterize the HW events; ii) derive a catalogue of subtropical ridges; iii) identify SIs, as explained next.

2.2. Spatio-temporal heatwave detection

To characterize the 2018 and 2019 HWs, we have adopted a semi-lagrangian perspective, following the methodology developed recently by Sánchez-Benítez et al. (2018) for the diagnosis of HW events. This methodology focuses on the spatio-temporal evolution of extreme temperature patterns (using the 850 hPa temperature, T850), instead of considering HWs as isolated local surface extremes. This enables the temporal monitoring of the spatial extent of HWs affecting distinct areas during their life cycle. The algorithm identifies HW events, defined as areas larger than 500,000 km^2 with daily mean T850 above the local daily 95th percentile (with respect to 1981–2010) that persist for at least 4 consecutive days. Additional information on this methodology can be found in Sánchez-Benítez et al. (2018).

2.3. Subtropical ridge catalogue

Here, a subtropical ridge catalogue (Sousa et al., 2018) was used to characterize the large-scale atmospheric circulation during the HW events. Subtropical ridges are diagnosed as regions between 35° and 55°N displaying more than 75% of the grid points above the 80th percentile of the Z500 climatological fields, while no more than 50% of grid points located further north surpass that threshold (to avoid overlaps with high-latitude blocking). Following the climatological assessments of Sousa et al. (2018), ridges occurring between 15°W and 15°E were considered. Specific details on the detection algorithm and the derived catalogue can be found in the abovementioned work.

2.4. Saharan air mass classification

A classification of air masses originated at low latitude subtropical desertic areas was performed relying on simple thermodynamical air properties: the 1 000-500 hPa layer geopotential thickness (Galvin, 2016) and the mean 925-700 hPa layer potential temperature (θ). Based on the climatological (1948–2018) mean summer (June–August) values of these variables for each grid point, the following conditions were considered to identify air masses of subtropical origin:

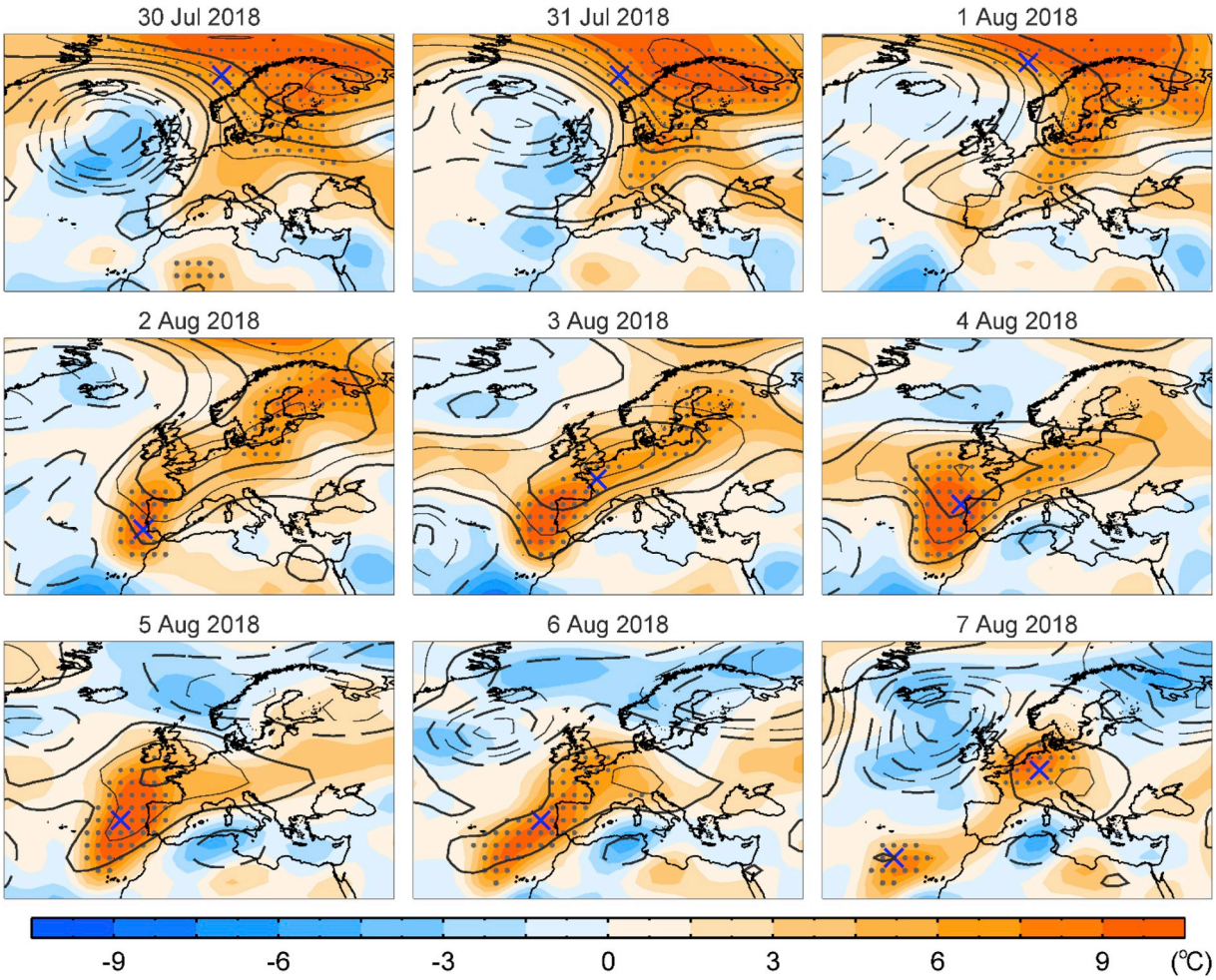

Fig. 3. Daily anomalies of temperature at 850 hPa (°C, shading) and geopotential height at 500 hPa (m, contours, with contour interval of 40 m starting at ±40 m and solid/dashed contours indicating positive/negative anomalies) between 30 July and 7 August 2018, using the NCEP/NCAR reanalysis dataset. Dots identify regions under heatwave conditions according to our algorithm, with blue crosses displaying the mass center of each heatwave pattern, which is defined as the averaged longitude and latitude of the gridpoints displaying heatwave conditions, weighted by the amplitude of the temperature anomalies. (For interpretation of the references to color in this figure legend, the reader is referred to the Web version of this article.)

i) 1 000-500 hPa thickness > 580 decameters (Galvin, 2016);
ii) 925-700 hPa $\theta > 40$ °C.

Grid points satisfying both criteria correspond to low density, warm, stable and very dry air masses, with the potential to be additionally warmed by downward advection processes (Wallace and Hobbs, 2006). This approach allows us to classify the mean climatological location and extension of desertic air masses for all summer days, as well as to identify temporary intrusions towards higher latitudes (e.g. the Iberian Peninsula) on a daily basis. In particular, SIs are detected over western (eastern) Iberia when the abovementioned criteria are verified in grid points north of 35°N and between 15°W-5°W (5°W-5°E). Note that some SIs can affect both sectors of Iberia simultaneously. Additionally, the longitudinal position of each SI was also computed on a daily basis, by searching for the longitude with the maximum value of geopotential thickness.

3. The record breaking events of August 2018 and June 2019

Several European areas (~6%) registered new absolute maximum temperature values during the June–August 2018 period (Fig. 1a), with a mean observed anomaly in Europe of ~+1.8 °C (Supplementary Fig. S1a), according to the E-OBS dataset. While records occurring in June 2018 were restricted to the British Isles, larger areas in Scandinavia and central Europe registered new extreme values throughout the remaining summer months. In particular, August 2018 stood out by the extreme conditions observed in western Iberia, as observations from this dataset indicate a large record-breaking area the region, with several stations registering values higher than 45 °C (Fig. 1a). Unprecedented values were mainly confined to continental Portugal, contrasting with the mean summer anomaly in this region, which was close to zero (Supplementary Fig. S1a). To analyze in more detail the exceptionality of the event and frame it in the historical context we used temperature observations from the Portuguese Met Office station network.

The average daily maximum, minimum and mean daily air temperature values for continental Portugal during the 2018 summer (formed from a representative set of eighty meteorological stations from IPMA) are presented in Fig. 2a. Extreme conditions occurred in early August 2018, following a sudden rise in temperatures. Prior to the event, temperatures were near-normal or slightly below average, except for a warm episode in mid-June. The warmest spell at national level occurred from 2 to 4 August, when the maximum temperature averaged for mainland Portugal exceeded 40 °C and daily mean temperatures were above the climatological mean of the maximum temperatures. During 1–6 August, more than half of the stations reached values above 40 °C and 17 stations registered values higher than 45 °C (IPMA (Instituto Português do Mar e da Atmosfera, 2018). As a consequence, 43 stations broke their previous historical maximum temperatures in Portugal (circa 40% of the

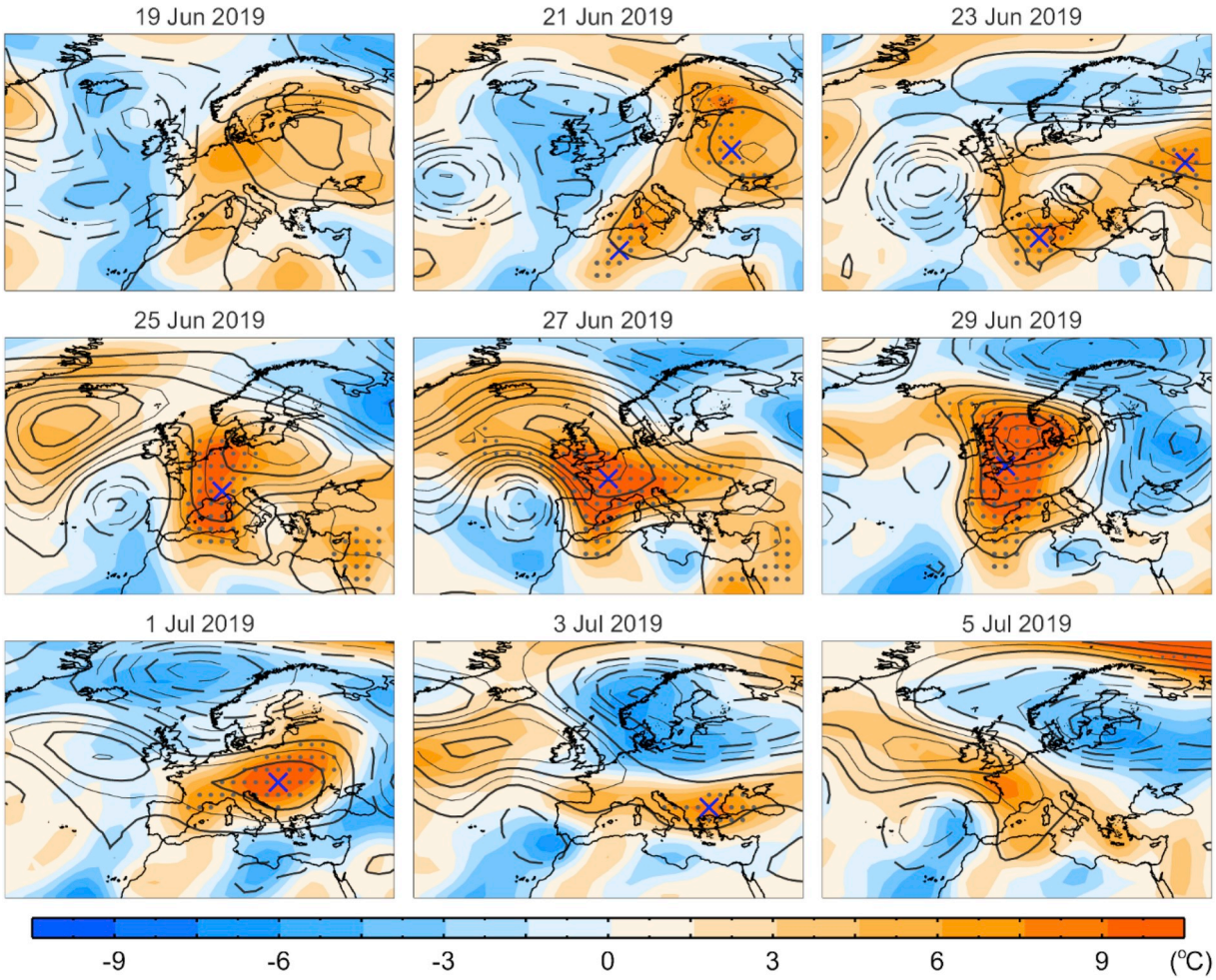

Fig. 4. As Fig. 3 but for the 2019 event, between 19 June and 5 July 2019, every two days.

country's official observation network) (see Fig. 2b). Also, ~30% of the Portuguese stations registered their all-time highest minimum temperature during that period.

The highest values (>45 °C) were observed relatively close to the westernmost sectors of Iberia, in pre-coastal central Portuguese provinces. In Fig. 2c the temperature exceedance over the previous records is also presented, highlighting the exceptionally of the event. Taking Lisbon - the capital of Portugal - as an example, the previous record of 42.0 °C (established during August 2003) was surpassed by 2 °C, setting a new absolute value of 44 °C. These results reinforce the more extreme, yet shorter-lived, nature of the 2018 episode over western Iberia, when compared to the less extreme, but longer-lived two-week event in 2003. Despite being relatively short-lived, the 2018 August event was so intense that it contributed decisively to place that month as the second warmest August on record in the country (after 2003) in terms of mean air temperature, and the warmest month ever in terms of maximum temperature, with a mean value of 32.4 °C (+3.6° anomaly).

Differently to the more regional 2018 event, the late June 2019 HW was long-lasting and affected different European regions between late June and early July, contributing to set the hottest June ever recorded in Europe, with a mean temperature anomaly of ~+2.3 °C with respect to 1981–2010. New records in maximum temperature were shattered across Europe (~4%) during June alone, mostly France and Spain, but also Switzerland, Germany, the Czech Republic or Poland (Fig. 1b). Extreme temperatures also occurred across central Europe later in July 2019, expanding the percentage of summer record-breaking European areas, although full summer data is not yet available at the time of this publication. In southwestern Europe, the HW peaked during 24–30 June, when temperatures were up to ~ l0°C above normal over some areas of France and Spain. It was the first time temperatures exceeded 45 °C in France, where the HW was made at least five times more likely as a result of anthropogenic climate change (Oldenborgh et al., 2019). Unlike the 2018 HW, the Spanish named "*hell-is-coming*" event of June 2019 registered the highest temperature anomalies in northeastern Iberia (Fig. 1b), where local temperatures climbed to more than 43 °C. Comparatively, southwestern Iberia was less affected by this HW, displaying weak temperature anomalies during that period. As this is also the climatological warmest region of Spain and Portugal, the 2019 event did not leave new all-time national records. In addition, the 2019 event was preceded by a cold temperature episode by mid-June, more intense over western Iberia, which contributed to lower the monthly mean temperatures therein (Fig. S1b). Due to these spatially and temporally contrasting temperatures, June 2019 was not among the warmest months on record for Spain and Portugal. Still, the Spanish Meteorological Agency (hereafter AEMET) recorded the warmest maximum temperatures of June in 29 stations of the main network including major cities such as Madrid and Barcelona (AEMET, 2019). New all-time absolute records were also set in five of these stations (some of them having data back to 1920), with temperature exceedances over their previous records of up to 3 °C. Interestingly, before this event only seven Spanish stations had their all-time maximum temperatures in June, some of them corresponding to the June 2017 event. Regarding minimum temperatures, 10 stations in Spain reported new records for June, and two of them saw their warmest nights since records started, with minimum temperatures above 25 °C.

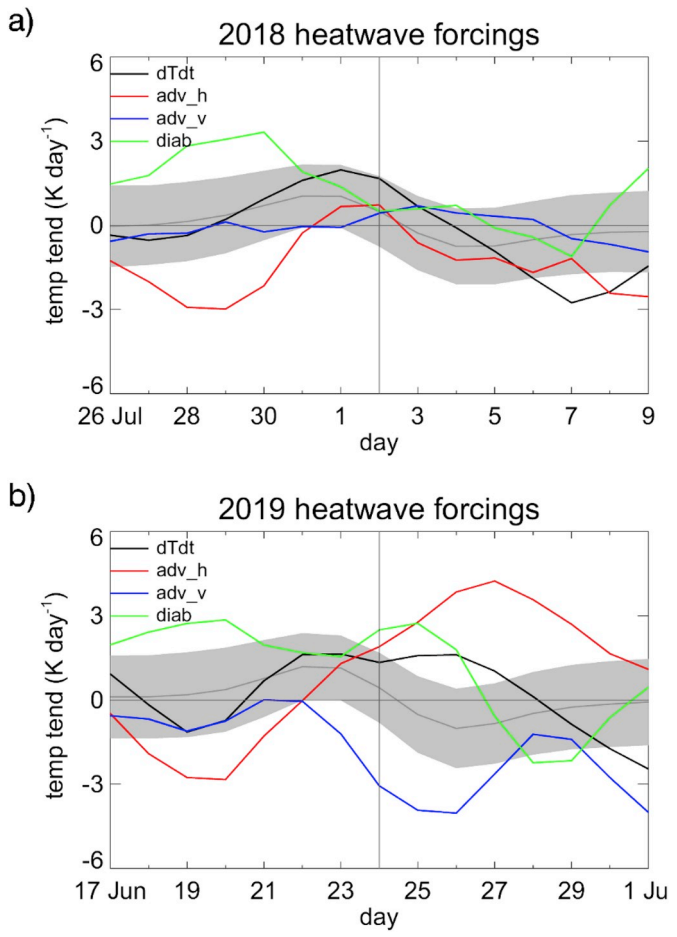

Fig. 5. Daily evolution of the 1 000-850 hPa mean temperature tendency (dTdt, black line) and its contributors (colored lines) (in K day^{-1}) from lag −7 to +7 days of the: a) August 2018 heatwave event; b) June 2019 heatwave event. These terms were averaged over land gridpoints of a) western Iberian Peninsula ([7.5, 5]°W and [37.5, 42.5]°N) and b) eastern Iberian Peninsula ([2.5, 0]° W and [37.5, 42.5]°N), using the NCEP/NCAR reanalysis dataset. Thermodynamical factors include horizontal (adv_h, red) and vertical (adv_v, blue) advection and diabatic processes (diab, green). Grey shading indicates the ±1 σ for temperature tendency as obtained from all 1948–2017 summer heatwave events that affected western/eastern Iberia. The vertical line represents the first day of the event over Iberia. A 3-day smoothing is applied to the series. (For interpretation of the references to color in this figure legend, the reader is referred to the Web version of this article.)

4. Regional atmospheric circulation

4.1. Evolution of the heatwaves

In this section, the spatio-temporal evolution of the IP HWs is examined, from prior to onset until the decaying phase, as shown in the panels of Figs. 3 and 4. Both events displayed some similarities, including the occurrence of a high-low pressure dipole over north-eastern Europe-eastern Atlantic. In the case of the 2018 HW, a persistent blocking event occurred in Scandinavia throughout July 2018, which was accompanied by extreme conditions over large parts of central and northern Europe (top panels of Fig. 3). At this stage, the positive Z500 anomaly associated with the block extended towards southwestern Europe, prompting the start of the warm Iberian event. By early August, the IP was affected by a subtropical ridge (detected in our ridge catalogue between 2 and 6 August). During the same period, the Z500 anomaly associated with the Scandinavian blocking cut-off, being later re-fed by the split of the Iberian ridge in two structures, due to a low-pressure system west of the British Isles. The HW algorithm detected an event between 2 and 7 August affecting a widespread area between the Madeira archipelago offshore Morocco and southeastern Scandinavia. For this 6-day period, the land area experiencing the highest number of days with HW conditions was western IP, where extreme temperatures persisted for 5 consecutive days (between 2 and 6 August, see Supplementary Fig. S2a).

Regarding the late June 2019 HW, it was also preceded by a high pressure system and extreme heat over northeastern Europe (top panels of Fig. 4). This positive Z500 anomaly center merged with another one that had already prompted HW conditions in northern Africa and extended towards the northeast as a subtropical ridge (detected between 22 and 30 of June). By 24 June, both centers merged over the western Mediterranean. Similar to the 2018 HW, the low-pressure system located over the eastern Atlantic stretched and intensified the subtropical ridge. However, in the 2019 HW, the Atlantic low was unusually displaced to the south, which allowed the high pressure system of central Europe to merge with an Atlantic blocking, extending HW conditions to the UK. The deepening of the Atlantic low occurred timely with the intensification and westward shift of a Siberian low-pressure system towards Scandinavia by the end of June (middle panels of Fig. 4), which contributed to set the subtropical ridge over western Europe. The last stage of the 2019 HW (bottom panels of Fig. 4) featured a transient evolution towards southeastern Europe, coinciding with the northward shift of the Scandinavian low. The HW algorithm detected a long-lasting event between 20 June and 3 July affecting large areas of Europe, from Ireland to Turkey and from the Mediterranean to southern Scandinavia. During this 14-day period, eastern IP, France, the Benelux or Switzerland were among the most affected regions, recording extreme temperatures for more than 7 days (see Fig. S2b). The outstanding intensity, duration and spatial extent of the 2019 HW are comparable to those typically observed during European mega-HWs (Sánchez-Benítez et al., 2018).

To address the relative role of distinct thermodynamical factors, we quantified the contribution of the horizontal/vertical temperature advection and diabatic processes to the temperature tendency over western and eastern IP during their respective HW events, by using the approach described in Sousa et al. (2018). The temporal evolution of these three terms in the period spanning 7 days before and after the HW onset over Iberia (2 August 2018 and 24 June 2019, respectively) is presented in Fig. 4. Again, despite some specificities of each episode, it is important to stress that both HW events showed similarities. Prior to the HWs, a balance between cold horizontal advection and diabatic heating maintained temperatures relatively stable. In the case of the 2018 HW, this was probably enhanced by the typical summer land-sea breeze circulation (e.g. Soares et al., 2014). A large and sustained increase in horizontal temperature advection was observed three days prior to the onset of the HWs over the IP, and became positive the day before. This was mainly due to the northward advection of a warm air mass towards the IP (see the poleward migration of warm anomalies from northern Africa to Iberia in the top panels of Figs. 3 and 4). This is a typical fingerprint of SIs, which also transport significant volumes of dust and other aerosols to mid latitudes. The occurrence of a SI during both HW events is further supported by satellite imagery (Supplementary Fig. S3) illustrating large amounts of dust over western and eastern Iberia.

Since the early stages of the 2018 HW, the advected Saharan air mass got “trapped” over western Iberia around an anticyclonic vortex (as shown in Supplementary Fig. S4). Accordingly, during most of this event, vertical temperature advection (suggesting enhanced subsidence) contributed to maintain the high temperatures against cold horizontal advection, which was present since 3–4 August 2018 (Fig. 5a). This westerly horizontal advection, carrying cooler Atlantic air, was the main responsible for the return to near-normal conditions over western Iberia in the 2018 HW event. Differently, vertical temperature advection was predominantly negative over eastern Iberia during the 2019 HW (Fig. 5b). As compared to the 2018 HW, the reduced contribution of this

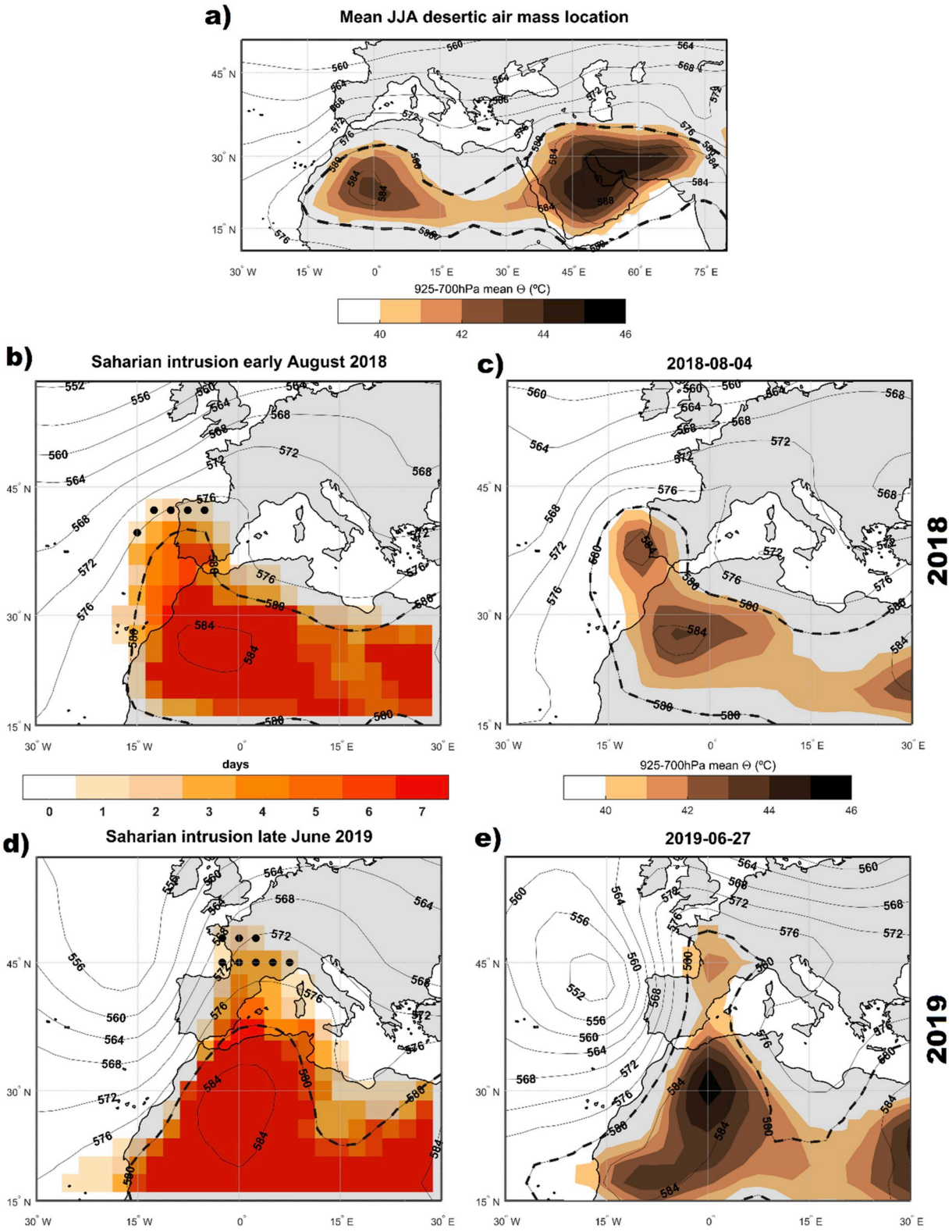

Fig. 6. a) Mean location and extension of typical desertic subtropical air masses during summer (JJA) computed for the period 1948–2018, with shaded values depicting the mean potential temperature in the 925-700 hPa layer, and the dashed black line limiting the area with 1 000–500 hPa thickness above 580 dam. b, d) Number of days (shaded) when the Saharan intrusion was detected in each gridpoint between b) 1 and 7 August 2018 and d) 24 and 30 June 2019. Black dots represent areas where such intrusions were unprecedented. Lines depict the composite for the 500 hPa geopotential height for the days when our algorithm detected heatwave conditions over Iberia. c, e) Same representation as in a), but for: c) 4 August 2018; e) 27 June 2019. The NCEP/NCAR reanalysis dataset was used for the identification of Saharan intrusions.

Table 1
Top 15 summer days (since 1948, using the NCEP/NCAR reanalysis dataset) averaged over western Iberian Peninsula (a, between 15°W-5°W) and eastern Iberian Peninsula (b, between 5°W-5°E) for: the mean 925-700hPa potential temperature (in °C); 850hPa level temperature (in °C).; the 1000-500hPa geopotential height thickness (in dam). Days of the early August 2018 and late June 2019 heatwave events in western/eastern Iberia are highlighted.

a)	Western Iberian Peninsula					
Rank	***Date***	$\Theta_{925\text{-}700hPa}$ ***(°C)***	***Date***	T_{850hPa} ***(°C)***	***Date***	$Thick_{850\text{-}500hPa}$ ***(dam)***
# 1	**2018-08-04**	**41.4**	**2018-08-04**	**26.8**	**2018-08-03**	**583**
# 2	**2018-08-03**	**40.7**	**2018-08-03**	**26.4**	**2018-08-04**	**582**
# 3	**2018-08-05**	**40.3**	**2018-08-05**	**25.8**	**2018-08-02**	**582**
# 4	2003-08-02	39.6	1995-07-24	25.8	**2018-08-05**	**581**
# 5	2003-08-01	39.4	2005-08-07	25.4	2017-08-20	580
# 6	1995-07-24	39.4	2003-08-02	25.4	2016-08-07	580
# 7	**2018-08-06**	**39.2**	**2018-08-02**	**25.2**	2013-07-07	580
# 8	2012-08-10	39.1	2003-08-01	25.1	2003-08-01	580
# 9	**2018-08-02**	**39.0**	1981-06-14	25.0	2005-08-05	580
# 10	2005-08-06	38.9	2005-08-06	25.0	1995-07-24	580
# 11	1981-06-14	38.9	2017-06-17	24.7	2005-08-06	580
# 12	2013-07-07	38.8	**2018-08-06**	**24.7**	1998-08-05	580
# 13	2012-06-26	38.8	2012-08-10	24.7	1998-08-06	580
# 14	1995-07-23	38.8	2012-06-26	24.7	2005-08-07	580
# 15	2005-08-05	38.7	2013-07-07	24.6	1998-08-06	580
b)	**Eastern Iberian Peninsula**					
Rank	***Date***	$\Theta_{925\text{-}700hPa}$ ***(°C)***	***Date***	T_{850hPa} ***(°C)***	***Date***	$Thick_{850\text{-}500hPa}$ ***(dam)***
# 1	1987-08-16	41.8	**2019-06-26**	**27.6**	1987-08-16	583
# 2	1980-08-03	41.8	1987-08-16	27.5	2005-07-17	583
# 3	1994-08-22	41.8	1987-08-15	27.3	1983-07-30	583
# 4	2005-07-17	41.8	1983-07-30	27.2	1980-08-02	583
# 5	1994-08-23	41.7	2005-07-17	27.2	2001-08-01	582
# 6	1987-08-15	41.6	1980-08-02	27.2	1980-08-03	582
# 7	1994-07-04	41.4	**2019-06-27**	**27.0**	1987-08-15	582
# 8	1980-08-02	41.4	2012-08-18	26.9	2005-07-16	582
# 9	2009-07-23	41.3	1982-07-07	26.8	2017-07-31	582
# 10	1983-07-30	41.2	1987-08-14	26.8	**2019-06-26**	**582**
# 11	2003-07-22	41.2	1994-08-22	26.8	1994-08-22	582
# 12	1982-07-07	41.1	1994-07-04	26.8	2015-07-27	582
# 13	2009-07-22	41.1	2005-07-16	26.6	2009-07-23	582
# 14	2009-07-24	41.0	1983-07-31	26.6	2017-08-01	581
# 15	2017-08-01	41.0	1999-08-25	26.6	2017-08-03	581

term is in agreement with a relatively larger dispersion of dust (Supplementary Fig. S5), the poleward location of the largest Z500 center anomaly (and associated regional maximum in subsidence) and the unusual shift of the Atlantic low towards the southeast (Fig. 4). Although the vertical term acted against the temperature rise, its effect was overwhelmed by the warm horizontal advection and the diabatic warming, which sustained the temperature increase during the first days of the late June 2019 HW (coinciding with the reorganization and intensification of the subtropical ridge). Warm advection was unusually intense and persisted several days after the onset of the 2019 HW over eastern Iberia, thus explaining the longer duration of this event, as compared to that of 2018.

The temperature tendency during the build-up of the early August 2018 HW exceeded the 1-sigma level associated with the climatology of all August HWs affecting western IP (not shown), and it was close to that threshold when considering all summer HWs over western IP (Fig. 5a). The temperature tendency during the late June 2019 HW was well beyond the 1-sigma level of all summer eastern IP HWs, mainly during the first days of the HW. In both cases, these exceptional values were largely due to the contribution of the horizontal advection term. As such, in the next subsection we turn our attention to this warm air advection from lower latitudes by focusing on the assessment of the SIs.

4.2. Unprecedented magnitude of the Saharan air mass intrusions

As displayed in Fig. 5, the onset of the IP HWs was prompted by the advection of an air mass that originated in the desertic areas of northern Africa. At this point, we aim to characterize some of the thermodynamical features of these air masses. Accordingly, we identified air masses with desertic characteristics for all summer days from June 1948 to June 2019, following the methodology described in Section 2.4. Fig. 6 shows the climatological characteristics of such air masses (Fig. 6a) and the corresponding daily fields for the 2018 (Fig. 6b–c) and 2019 (Fig. 6d–e) episodes.

Our classification highlights air masses usually located over northern Africa and the Middle East, as shown in Fig. 6a. There are two preferred areas for the development of stable, dry and warm air masses, namely western Sahara and the Arabic Peninsula. The typical summer geopotential thickness field displays a meridional gradient north of those areas, leading to a mean southwesterly flow in the vicinity of the IP that tends to keep desertic air masses relatively distant from the region, especially in westernmost sectors. Nevertheless, disruptions of this usual synoptic configuration (in particular those favoring southeasterly wind components) can be responsible for a northward intrusion of these air masses (e.g. Salvador et al., 2014).

The analyzed HW events featured a persistent and pronounced latitudinal extension of the 580 dam isohypse from western Sahara, as shown in Fig. 6b,d, indicating the occurrence of a SI. The full tracking of these SIs is shown in Supplementary Figs. S6 and S7. During their early stages, the potential temperature of the air mass was clearly above the climatological mean over the genesis region (northwestern Africa), stressing their remarkable thermodynamical properties. At the peak of the HW events, the very warm dry air was transported towards western (Fig. 6c) and eastern (Fig. 6e) IP. Figs. S6 and S7 evidence that the anomalous location of the Atlantic low pressure system fostered the northward displacement of the air masses towards Iberia. These SIs reached unusual northern latitudes in western and eastern IP, where they partially cut-off with outstanding intensity (Fig. 6c,e), matching the area of the most extreme surface temperatures.

The trapping of these SIs occurred further north of other SIs associated with relevant HWs in western and eastern IP. This is shown in Supplementary Fig. S8, which illustrates the SIs associated with other historical extremely warm episodes that affected western and eastern Iberia. Some similarities with the August 2018 and June 2019 events are found in the synoptic environment, in particular the deformation of the thickness field with a zonal gradient immediately west of the SI. This

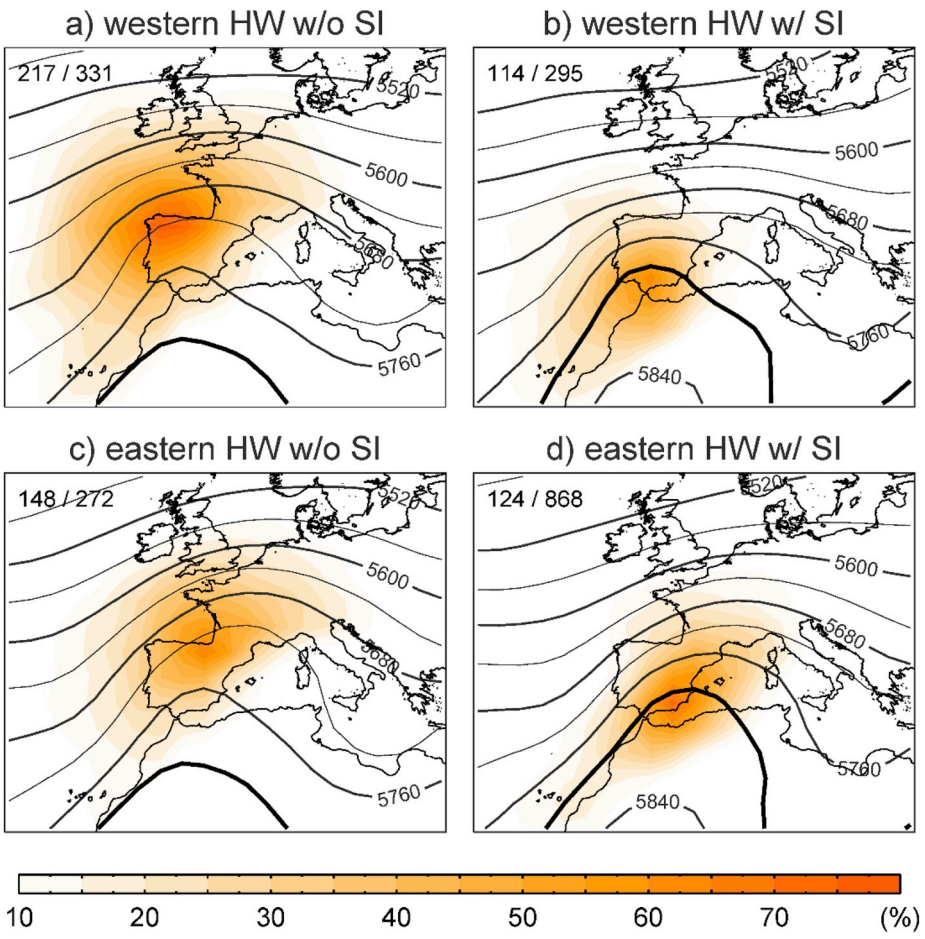

Fig. 7. Composites of 1 000–500 hPa geopotential height thickness (contours, in m) and local heatwave frequency (shading, in percentage of the total number of heatwave days) for: (a,c) Iberian heatwave days without Saharan intrusions; (b,d) Iberian heatwave days with Saharan intrusions, over (a,b) western and (c,d) eastern Iberia. Thick contour highlights the 580 dam thickness threshold employed in the identification of Saharan intrusions. The number of cases in each composite is shown in the upper left corner of each panel. The numbers after the slash indicate the total number of (a,c) heatwave and (b,d) Saharan intrusion days in (a,b) western and (c,d) eastern Iberia. The NCEP/NCAR reanalysis dataset was used for the identification of Saharan intrusions.

configuration favors a south-north flow that is often associated with a low pressure system or a mid-tropospheric trough in the eastern Atlantic. In fact, this feature appears to play a critical role to initiate an anomalous poleward advection of the relatively stationary warm air mass located over northern Africa. Despite these commonalities, the visual analysis of the maps supports that: i) the SIs reached unprecedented latitudes over western and eastern IP at the peak of the August 2018 and late June 2019 HW events (actually, they extended further north than any other SI of the reanalysis period, Fig. 5b,d); ii) a significant fraction of major IP HWs are related to SIs. The latter will be further assessed in the next section.

5. The relevance of Saharan intrusions in the Iberian Peninsula

5.1. Regional contribution to heatwave events

To objectively classify the level of exceptionality of the 2018 and 2019 SIs, as well as the relevance of SIs to extreme heat episodes, we ranked all summer days since 1948 based on the highest values of the following indicative variables (averaged over western and eastern IP separately): a) 925-700 hPa mean layer potential temperature; b) 850 hPa temperature; c) 1 000-500 hPa geopotential height thickness.

The analysis of these three rankings clearly places the 2018 HW as the most extreme event in western IP. In fact, the warmest day of the HW event (4 August 2018) is ranked first in 925–700 hPa mean layer potential temperature and 850 hPa level temperature, and the days spanning between 2 and 6 August 2018 also dominate these rankings, overwhelming past extreme days by a large margin (Table 1a). Other historical HW events (as presented in Supplementary Fig. S8) with important socio-economic impacts in western IP (e.g. 1981 or 2003–[24] Trigo et al., 2009) are also listed within the top-15 of the ranking. This matching shows how SIs are frequently related to extreme heat episodes in western IP. A similar ranking analysis is presented for eastern IP in Table 1b. Despite being the strongest event ever occurring in the western sector, the 2018 episode falls well below other previous events in eastern IP, not being ranked even in the top-15. When both sectors are compared, the exceptionality of recent episodes (since 2000) is considerably more noticeable in western IP, while there is a larger fraction of pre-2000 events in the eastern IP rankings. The latter suggests some decadal variability in the intensity of SIs. In spite of this, the intense June 2019 episode also appears in the top-15 ranking of eastern IP SIs for 850 hPa temperature and 850-500 hPa geopotential height thickness, being listed first for the former diagnostic.

The results of Table 1 highlight differences between western and eastern IP SIs. To analyze in more detail these regional differences in the relationship between the occurrence of HWs and SIs, we derived a catalogue of regional HWs and SIs for each half of the IP, using the west-east division based on the 5°W meridian. HW events were compared against SIs for each sector separately (Fig. 7), thus enabling a better comprehension of the relevance of SIs to regional IP HWs.

A SI was detected in ~1/3 of western IP HWs (114 out of 331). This relationship becomes much stronger in the southern half of western IP, where SIs are responsible for more than half of HWs (shading in Fig. 7b), whereas northwestern IP HWs are more often unrelated to such intrusions (Fig. 7a). Consequently, the relevance of SIs to western IP HWs increases southwards. A similar north/south preference is found for eastern IP HWs without/with SI (Fig. 7c–d). This is not surprising, considering the common restriction of such intrusions to areas south of ~40°N, only broken by the unprecedented 2018 and 2019 events (Section 4.2). For both regions, there is also a clear difference in the

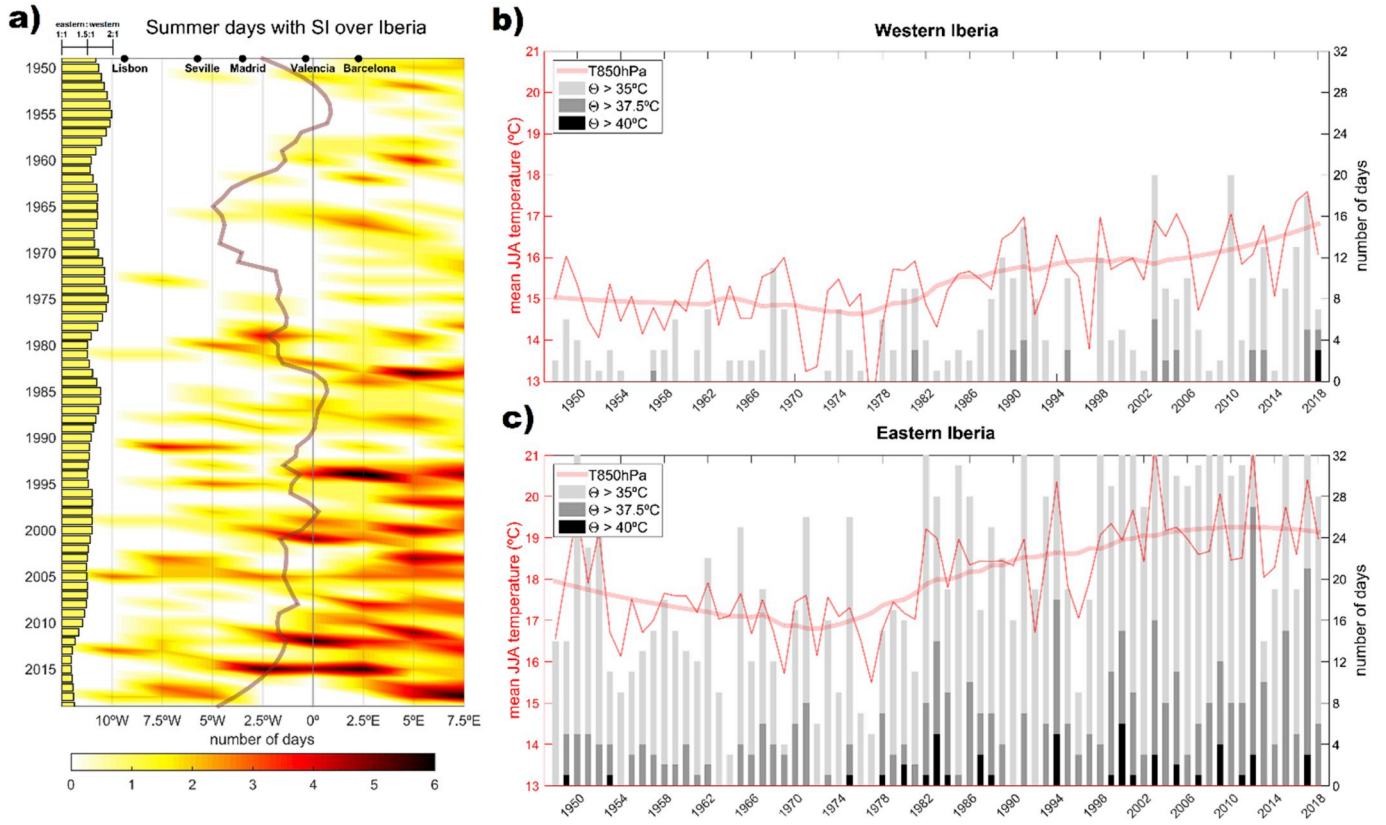

Fig. 8. a) Hovmoller diagram representing the long-term evolution in the number of SIs affecting the Iberian Peninsula (shading). The location of SIs is assigned based on the longitude of its maximum intensity. The reddish thick line represents the evolution in the mean longitudinal position of subtropical ridges occurring within 15°W-15°E. The yellow bars in the left represent the ratio between the frequency of SIs in eastern and western Iberia. b) Inter-annual variability of the mean summer 850 hPa temperature (thin red line), its smoothed 30-year-mean (thick red line), and of the frequency of days with the 925-700 hPa mean layer potential temperature above different thresholds (grey bars) in western Iberia (between 15°W-5°W). c) Same as b), but for eastern Iberia (between 5°W-5°E). The NCEP/NCAR reanalysis dataset was used for the identification of Saharan intrusions. (For interpretation of the references to color in this figure legend, the reader is referred to the Web version of this article.)

northward penetration of extremely thick layers between HWs with and without SI (cf. thick lines in Fig. 7). However, the ratio of SIs causing HWs in these regions is quite different. Overall, SIs are more frequent over central Mediterranean areas (Salvador et al., 2014) and hence they are more prone to occur in eastern (868 cases) than western (295) sectors of the IP. However, SIs towards eastern IP are often characterized by an accentuated SW-NE tilt in the mean position of the 580 dam, which favors HWs in central Mediterranean, with little incidence in eastern IP. As a consequence, the total number of SIs causing HWs is similar in western and eastern sectors, but the probability of a SI to trigger HW conditions is higher in western IP.

5.2. Long-term variability

Taking into account the links between IP HWs and SIs reported above and the increasing frequency of IP HWs in the last decades, it is important to assess long-term changes in the characteristics of SIs. In this section changes in the frequency of SIs during the 1948–2018 period are explored, by diagnosing long-term trends in (Fig. 8): i) the number of days with SI; ii) the number of days with mean 925-700 hPa θ above several thresholds; iii) the mean summer T850.

Fig. 8a shows a marked increase in the number of SIs since 1948. Years where more than 6 SIs have been registered have become relatively frequent in the last 3 decades, in contrast with the much smaller frequencies observed prior to this. As discussed above, eastern IP is more prone to such intrusions, when compared to western IP, as also inferred from the frequencies of 925–700 hPa mean θ presented in Fig. 8b–c. Both sectors present a noticeable increase in the frequency of exceedance for different θ thresholds, in particular since the mid-1970s, albeit the steep increase seems to be attenuated in the eastern sector after 2000 (Fig. 8c). Differently, the increase of SI-related properties in western IP has remained unabated and even accelerated since the turning of the century (Fig. 8b). As a consequence, and despite the occurrence of the outstanding June 2019 event, the frequency of western IP SIs relative to that of eastern IP has increased in the last years (see the ratio of eastern vs western SIs in the yellow bars of Fig. 8a). A similar behavior occurred in the mid-1960s and the 1970s, when a slightly decrease of SIs occurred in eastern but not in western IP. Interestingly, these anomalous periods have been accompanied by zonal shifts in the mean location of subtropical ridges (thick line in Fig. 8a), with westward migrations of these systems concurring with relative increases in western IP SIs. Overall, the corresponding evolution of the ratio between eastern and western SIs shown in Fig. 8a (yellow bars) supports this. These results suggest that, superimposed on the long-term trends, there are inter-decadal fluctuations in the relative frequency of western vs eastern IP SIs apparently mediated by subtropical ridges. The SI-ridge link is supported by the fact that SIs are typically embedded within subtropical ridges, which have been associated with the occurrence of extreme heat episodes in southern Europe, particularly over the IP (Sousa et al., 2018).

Note that the abovementioned west-east shifts in the occurrence of SIs simply appear as modulating factors of the long-term trends and hence they are compatible with the occurrence of record-breaking events in any of the regions. To stress this, local trends in the summer frequency of SIs since 1948 have been computed (Fig. 9a). The results confirm the generalized increase of SIs reported in Fig. 8, which is

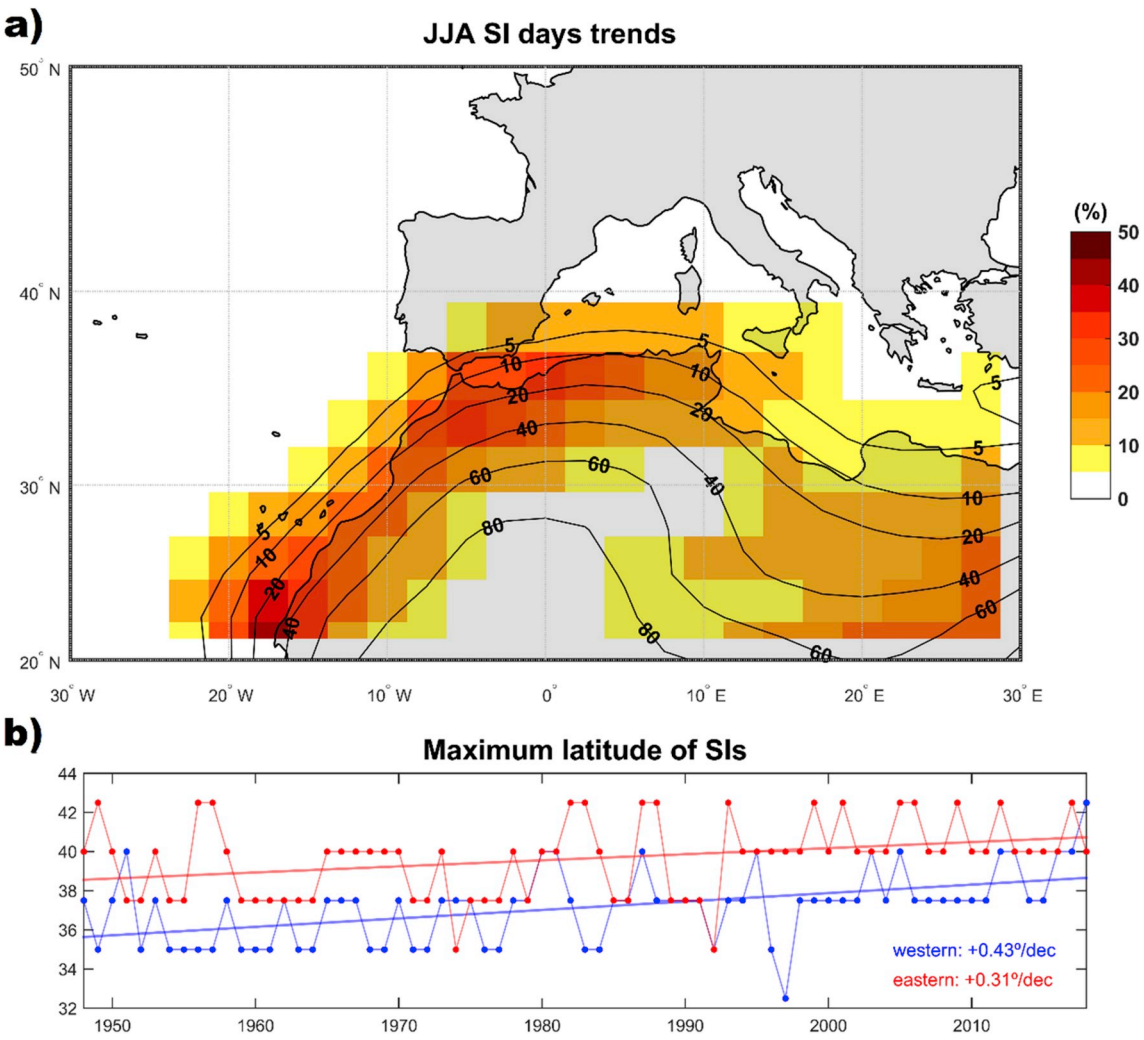

Fig. 9. a) Changes in the relative frequency of summer days with the presence of Saharan air masses (shaded) since 1948, using the NCEP/NCAR reanalysis dataset. Black lines represent the mean climatological absolute frequencies. b) Trends for the yearly northernmost latitude of SIs in western (blue) and eastern (red) sectors of the Iberian Peninsula during the same period. Trends are statistically significant at the 95% confidence level. (For interpretation of the references to color in this figure legend, the reader is referred to the Web version of this article.)

particularly notable in areas where the climatological occurrence is relatively low (e.g., to the northwest of the Sahara desert), thus depicting a poleward expansion of desertic climates and associated air masses, in line with previous results (e.g. Thomas and Nigam, 2017). This is supported by the regional trends in the northernmost latitude reached by summer SIs in western/eastern IP (Fig. 9b), being the trend more notable in the western sector (+0.43°/decade). These long-term trends allow us to frame the exceptionality of the August 2018 and June 2019 SIs, which reached latitudes further north than those expected from their regional trends (particularly the 2019 event).

6. Discussion

In this work we have analyzed the heatwave events that affected the IP during early August 2018 and late June 2019. An analysis based on a semi-lagrangian HW tracking algorithm complemented the observational assessment of these events, which were unprecedented in terms of near-surface temperatures over western and eastern IP, respectively. Despite their differences (a short-lived 2018 HW vs a 2019 mega-HW), these extraordinary events were associated with a Saharan warm air intrusion over western and eastern IP, respectively. Both SIs occurred under a strong southerly flow prompted by a subtropical ridge and a low pressure system over the eastern Atlantic. This configuration led to anomalously warm tropospheric conditions associated with warm horizontal advection from subtropical latitudes, which is a well-known typical setup for the occurrence of HWs in the region (Trigo et al., 2006; Pereira et al., 2005; Tomczyk et al., 2017). The intensity and persistence of the warm advection episode largely determined the life-cycles of the August 2018 and June 2019 HWs, as well as their differences.

To better characterize SIs, we designed an approach that detects and classifies desertic air masses based on thermodynamical properties (1 000-500 hPa geopotential height thickness and potential temperature in the 925-700 hPa layer). Our results show that the poleward extension of the August 2018 and June 2019 SIs reached the northernmost latitudes of western and eastern IP, respectively, affecting areas where such intrusions had never been detected in the long-term record (since 1948). The anomalous extension of these SIs, together with their unprecedented intensities (in terms of temperature and/or geopotential height thickness) explains the exceptional meteorological observations. Actually, some of the characteristics of the SIs were unprecedented as compared to those registered during all previous HWs affecting western and eastern IP, including the outstanding episodes of 2003 and 2017.

Based on their exceptional signatures, the August 2018 and June 2019 events may be considered the most prominent and exemplificative links between the advection of a desertic air mass and extreme

temperatures in western and eastern IP, respectively. A more detailed assessment of these relationships reveals regional differences in the relevance of SIs to the occurrence of HWs for the two halves of the IP. Although SIs are more frequent in eastern IP (due to its geographical location), the incidence of HWs under SIs is similar in both sectors, making this mechanism more efficient in western IP. This seems to be related to the enhanced SW-NE tilt of SIs in the eastern sector.

We also report an increasing frequency of SIs over both eastern and western IP in the long-term record. This overall trend is in agreement with long-term thermodynamical changes (i.e. warming and expansion of the troposphere) related to global warming (Staten et al., 2018; IPCC, 2013; Lu et al., 2007), and with regional observational trends of extreme heat events in Portugal (Cardoso et al., 2018; Ramos et al., 2011) and Spain (Gonzalez-Hidalgo et al., 2015; del Rio et al., 2011). Superimposed on the long-term trend of SIs, our results also suggest multi-decadal variations in the relative frequency of such intrusions over western and eastern IP. This variability seems to act in concert with zonal shifts in the mean location of subtropical ridges affecting the IP, and modulates the regional trends of SIs. Accordingly, we report a recent steeper trend of SIs in western IP, and a relatively less marked trend in eastern IP. While in the former region, the most extreme SIs have occurred in the 21st century, in the latter numerous 20th century events still remain as top SIs, despite the occurrence of the June 2019 event. A deeper analysis of the links between SIs and subtropical ridges, the multi-decadal variability of SIs and the possible causes behind the zonal shifts in subtropical ridges should be performed in future studies.

Summing up, our results demonstrate that SIs play a critical role for the occurrence of HWs, particularly those affecting the southern sectors of the Iberian Peninsula. Although SIs are generally less relevant for northern IP HWs, the unprecedented latitude reached by the early August 2018 and late June 2019 events and the reported poleward trend of summer SIs anticipate an increasing role of SIs also in northernmost areas of the IP and other western European regions. Accordingly, there is a critical need for increased awareness and prevention about impacts related to public health issues (Achebak et al., 2018; Díaz, 2017), wildfires (Sousa et al., 2015) or drought management (Guerreiro et al., 2017; Páscoa et al., 2017), amongst other hazards directly or indirectly related with the abovementioned observed (and projected under global warming – IPCC, 2013) rising trend in extreme HWs, particularly under the Mediterranean environment (Fischer and Schär, 2010).

Acknowledgements

We acknowledge the E-OBS dataset from the EU-FP6 project ENSEMBLES (http://ensembles-eu.metoffice.com) and the data providers in the ECA&D project (http://www.ecad.eu). PMS was supported by project IMDROFLOOD [Improving Drought and Flood Early Warning, Forecasting and Mitigation using real-time hydroclimatic indicators (WaterJPI/0004/2014)] and project HOLMDRIVE [North Atlantic Atmospheric Patterns influence on Western Iberia Climate: From the Lateglacial to the Present (PTDC/CTA-GEO/29029/2017)] through Fundação para a Ciência e a Tecnologia, Portugal (FCT). RMT was partially supported by national funds through Fundação para a Ciência e a Tecnologia, Portugal (FCT) under project FireCast (PCIF/GRF/0204/2017). This work was partially funded by project INDECIS, which is part of ERA4CS, an ERA-NET initiated by JPI Climate, with co-funding by the European Union (Grant 690462). AMR was supported by the Scientific Employment Stimulus 2017 from FCT (CEECIND/00027/2017). We thank the Editor and reviewers for their helpful comments on this manuscript.

Appendix A. Supplementary data

Supplementary data to this article can be found online at https://doi.org/10.1016/j.wace.2019.100224.

References

Achebak, H., Devolder, D., Ballester, J., 2018. Heat-related mortality trends under recent climate warming in Spain: a 36-year observational study. PLoS Med. 15 (7), e1002617 https://doi.org/10.1371/journal.pmed.1002617.

AEMET, 2019. Informe Mensual Climatológico Junio de 2019 (in Spanish). Retrieved from. http://www.aemet.es/documentos/es/serviciosclimaticos/vigilancia_clima/resumenes_climat/mensuales/2019/res_mens_clim_2019_06.pdf.

Barriopedro, D., Fisher, E., Luterbacher, J., Trigo, R.M., García-Herrera, R., 2011. The hot summer of 2010: redrawing the temperature record map of Europe. Science 322, 220. https://doi.org/10.1126/science.1201224.

BBC News, 2019. European heatwave sets new June temperature records. Retrieved from. https://www.bbc.com/news/world-europe-48780685.

Cardoso, R.M., Soares, P.M.M., Lima, D.C.A., Miranda, P.M.A., 2018. Mean and extreme temperatures in a warming climate: EURO CORDEX and WRF regional climate high-resolution projections for Portugal. Clim. Dyn. 52 (1–2), 12, 2018. https://doi.org/10.1007/s00382-018-4124-4.

del Río, S., Herrero, L., Pinto-Gomes, C., Penas, A., 2011. Spatial analysis of mean temperature trends in Spain over the period 1961–2006. Glob. Planet. Chang. 78, 65–75. https://doi.org/10.1016/j.gloplacha.2011.05.012.

Díaz, J., Linares, C., Carmona, R., Russo, A., Ortiz, C., Salvador, P., Trigo, R.M., 2017. Saharan dust intrusions in Spain: health impacts and associated synoptic conditions. Environ. Res. 156, 455–467. https://doi.org/10.1016/j.envres.2017.03.047.

Dole, R., Hoerling, M., Perlwitz, J., Eischeid, J., Pegion, P., Zhang, T., Quan, X.W., Xu, T., Murray, D., 2011. Was there a basis for anticipating the 2010 Russian heat wave? Geophys. Res. Lett. 38, L06702. https://doi.org/10.1029/2010GL046582.

El Tiempo Hoy, 2018. La Aemet alerta: posible ola de calor en España a partir de la semana que viene. Retrieved fromhttps://www.eltiempohoy.es/elcielo/meteorologia/ola-de-calor-agosto-2018-aemet-alerta_0_2601375045.html. .

Fischer, E.M., Schär, C., 2010. Consistent geographical patterns of changes in high-impact European heatwaves. Nat. Geosci. 3 (6), 398–403. https://doi.org/10.1038/NGEO866.

Galvin, J.F.P., 2016. An Introduction to the Meteorology and Climate of the Tropics. Wiley-Blackwell, p. 328pp.

García-Herrera, R., Díaz, J., Trigo, R.M., Luterbacher, J., Ficher, E., 2010. A review of the European summer heat wave of 2003. Crit. Rev. Environ. Sci. Technol. 40, 267–306.

Gonzalez-Hidalgo, J.C., Peña-Angulo, D., Brunetti, M., Cortesi, N., 2015. Recent trend in temperature evolution in Spanish mainland (1951–2010): from warming to hiatus. Int. J. Climatol. 36, 2405–2416. https://doi.org/10.1002/joc.4519.

Guardian, The, 2019. Spain battles biggest wildfires in 20 years as heatwave grips Europe. Retrieved from. https://www.theguardian.com/world/2019/jun/27/hundreds-of-firefighters-tackle-blaze-in-north-east-spain.

Guerreiro, S.B., Kilsby, C., Fowler, H.J., 2017. Assessing the threat of future megadrought in Iberia. Int. J. Climatol. 37, 5024–5034. https://doi.org/10.1002/joc.5140.

Haylock, M.R., Hofstra, N., Klein Tank, A.M.G., Klok, E.J., Jones, P.D., New, M., 2008. A European daily high-resolution gridded dataset of surface temperature and precipitation. J. Geophys. Res. 113, D20119. https://doi.org/10.1029/2008JD10201.

IPCC, 2013. Annex I: Atlas of global and regional climate projections. In: van Oldenborgh, G.J., et al. (Eds.), Climate Change 2013: The Physical Science Basis. Contribution of Working Group I to the Fifth Assessment Report of the Intergovernmental Panel on Climate Change. ed T F Stocker. Cambridge University Press, Cambridge, New York.

IPMA (Instituto Português do Mar e da Atmosfera, I.P., 2018. Resumo Climatológico – Agosto de 2018.

Kalnay, E., Kanamitsu, M., Kistler, R., Collins, W., Deaven, D., Gandin, L., Iredell, M., Saha, S., White, G., Woollen, J., Zhu, Y., Chelliah, M., Ebisuzaki, W., Higgins, W., Janowiak, J., Mo, K.C., Ropelewski, C., Wang, J., Leetmaa, A., Reynolds, R., Jenne, R., Joseph, D., 1996. The NCEP/NCAR 40-year reanalysis project. Bull. Am. Meteorol. Soc. 77 (3), 437–471. https://doi.org/10.1175/1520-0477(1996)077<0437:TNYRP>2.0.CO;2.

Lu, J., Vecchi, G.A., Reichler, T., 2007. Expansion of the Hadley cell under global warming Geophys. Res. Lett. 34, L06805.

Miralles, D.G., Teuling, A.J., van Heerwaarden, C.C., de Arellano, J.V.G., 2014. Mega-heatwave temperatures due to combined soil desiccation and atmospheric heat accumulation. Nat. Geosci. 7, 345–349. https://doi.org/10.1038/ngeo2141.

Oldenborgh, G., et al., 2019. Human contribution to the record-breaking June 2019 heat wave in France. World weather attribution group. Retrieved from. https://www.worldweatherattribution.org/human-contribution-to-record-breaking-june-2019-heatwave-in-france/.

Páscoa, P., Gouveia, C.M., Russo, A., Trigo, R.M., 2017. Drought trends in the iberian Peninsula over the last 112 years. Adv. Meteorol. 2017, 4653126 https://doi.org/10.1155/2017/4653126.

Pereira, M.G., Trigo, R.M., DaCamara, C.C., Pereira, J.M.C., Leite, S.M., 2005. Synoptic patterns associated with large summer forest fires in Portugal. Agric. For. Meteorol. 129, 11–25.

Público, 2018. Poeiras vindas do Norte de África vão chegar a todo o país. Retrieved from. https://www.publico.pt/2018/07/31/sociedade/noticia/poeiras-vindas-do-norte-de-africa-vao-chegar-a-todo-o-pais-e-podem-agravar-problemas-respiratorios-1839639#gs (QGScOLWk).

Ramos, A.M., Trigo, R.M., Santo, F.E., 2011. Evolution of extreme temperatures over Portugal: reporting on recent changes and future scenarios. Clim. Res. 48, 177–192. https://doi.org/10.3354/cr00934.

Russo, S., Sillmann, J., Fischer, E., 2015. Top ten European heatwaves since 1950 and their occurrence in the coming decades. Environ. Res. Lett. 10, 054016 https://doi.org/10.1088/1748-9326/10/12/124003.

Salvador, P., Alonso-Pérez, S., Pey, J., Artíñano, B., de.Bustos, J.J., Alastuey, A., Querol, X., 2014. African dust outbreaks over the western Mediterranean Basin: 11-year characterization of atmospheric circulation patterns and dust source areas. Atmos. Chem. Phys. 14, 6759–6775. https://doi.org/10.5194/acp-14-6759-2014.

Sánchez-Benítez, A., García-Herrera, R., Barriopedro, D., Sousa, P.M., Trigo, R.M., 2018. June 2017: the earliest european summer mega-heatwave of reanalysis period. Geophys. Res. Lett. 45, 1955–1962. https://doi.org/10.1002/2018GL077253.

Schär, C.1, Vidale, P.L., Lüthi, D., Frei, C., Häberli, C., Liniger, M.A., Appenzeller, C., 2004. The role of increasing temperature variability in European summer heatwaves. Nature 427, 332–336. https://doi.org/10.1038/nature02300.

Soares, P.M.M., Cardoso, R.M., Semedo, A., Chinita, M.J., Ranjha, R., 2014. Climatology of the Iberia coastal low-level wind jet: weather research forecasting model high-resolution results. Tellus A Dyn. Meteorol. Oceanogr. 66. https://doi.org/10.3402/tellusa.v66.22377.

Sousa, P.M., Trigo, R.M., Pereira, M.G., Bedia, J., Gutiérrez, J.M., 2015. Different approaches to model future burnt area in the Iberian Peninsula. Agric. For. Meteorol. 202, 11–25. https://doi.org/10.1016/j.agrformet.2014.11.018.

Sousa, P.M., Trigo, R.M., Barriopedro, D., Soares, P.M.M., Santos, J.A., 2018. European temperature responses to blocking and ridge regional patterns. Clim. Dyn. 50, 457–477. https://doi.org/10.1007/s00382-017-3620-2.

Staten, P.W., Lu, J., GriseKM, Davis SMand Birner, T., 2018. Reexamining tropical expansion Nat. Clim. Change 8, 768–775. https://doi.org/10.1038/s41558-018-0246-2.

Thomas, N., Nigam, S., 2017. Twentieth-century climate change over Africa: seasonal HydroclimateTrends and Sahara desert expansion. J. Clim. 31, 3349–3370. https://doi.org/10.1175/JCLI-D-17-0187.1.

Tomczyk, A.M., Półrolniczak, M., Bednorz, E., 2017. Circulation conditions' effect on the occurrence of HeatWaves in western and southwestern Europe. Atmosphere 8, 31. https://doi.org/10.3390/atmos8020031.

Trigo, R.M., Pereira, J.M.C., Pereira, M.G., Mota, B., Calado, M.T., DaCamara, C.C., Santo, F.E., 2006. Atmospheric conditions associated with the exceptional fire season of 2003 in Portugal. Int. J. Climatol. 26 (13), 1741–1757.

Trigo, R.M., Ramos, A.M., Nogueira, P., Santos, F.D., García-Herrera, R., Gouveia, C.M., Santo, F.E., 2009. Evaluating the impact of extreme temperature based indices in the 2003 heatwave excessive mortality in Portugal. Environ. Sci. Policy 12, 844–854.

Wallace, J.M., Hobbs, P.V., 2006. Atmospheric Science – an Introductory Survey, second ed. Elsevier, Canada.